

Imaginary-time hierarchical equations of motion for thermodynamic variables

Cite as: J. Chem. Phys. **156**, 174112 (2022); <https://doi.org/10.1063/5.0091468>

Submitted: 15 March 2022 • Accepted: 18 April 2022 • Accepted Manuscript Online: 18 April 2022 •
Published Online: 05 May 2022

 Jiaji Zhang and  Yoshitaka Tanimura



View Online



Export Citation



CrossMark

ARTICLES YOU MAY BE INTERESTED IN

[Numerically “exact” approach to open quantum dynamics: The hierarchical equations of motion \(HEOM\)](#)

The Journal of Chemical Physics **153**, 020901 (2020); <https://doi.org/10.1063/5.0011599>

[Generalization of the hierarchical equations of motion theory for efficient calculations with arbitrary correlation functions](#)

The Journal of Chemical Physics **152**, 204101 (2020); <https://doi.org/10.1063/5.0007327>

[Unified treatment of quantum coherent and incoherent hopping dynamics in electronic energy transfer: Reduced hierarchy equation approach](#)

The Journal of Chemical Physics **130**, 234111 (2009); <https://doi.org/10.1063/1.3155372>

Lock-in Amplifiers
up to 600 MHz



Zurich
Instruments



Imaginary-time hierarchical equations of motion for thermodynamic variables

Cite as: J. Chem. Phys. 156, 174112 (2022); doi: 10.1063/5.0091468

Submitted: 15 March 2022 • Accepted: 18 April 2022 •

Published Online: 5 May 2022



View Online



Export Citation



CrossMark

Jiaji Zhang^{a)}  and Yoshitaka Tanimura^{a)} 

AFFILIATIONS

Department of Chemistry, Graduate School of Science, Kyoto University, Kyoto 606-8502, Japan

^{a)} Authors to whom correspondence should be addressed: zhang.jiaji.192@kyoto-u.jp and tanimura.yoshitaka.5w@kyoto-u.jp

ABSTRACT

The partition function (PF) plays a key role in the calculation of quantum thermodynamic properties of a system that interacts with a heat bath. The imaginary-time hierarchical equations of motion (imHEOM) approach was developed to evaluate in a rigorous manner the PF of a system strongly coupled to a non-Markovian bath. In this paper, we present a numerically efficient scheme to evaluate the imHEOM utilizing the β -differentiated imHEOM (BD-imHEOM) that are obtained by differentiating the elements of the imHEOM with respect to the inverse temperature. This approach allows us to evaluate the system, system–bath interaction, and heat–bath parts of the PF efficiently. Moreover, we employ a polyharmonic decomposition method to construct a concise hierarchical structure with better convergence, thus reducing the cost of numerical integrations. We demonstrate the proposed approach by compute thermodynamic quantities of a spin–boson system and a 2×2 antiferromagnetic triangular spin lattice system with an Ohmic spectral distribution.

Published under an exclusive license by AIP Publishing. <https://doi.org/10.1063/5.0091468>

I. INTRODUCTION

The Boltzmann principle and the maximum entropy principle are the central dogmas of statistical mechanics, and they allow us to compute the thermodynamic variables of a dynamical system, characterized by its temperature T . In the framework of canonical statistical physics, a widely used assumption is that of a heat bath interacting with the main system and yielding the system in its equilibrium state $\hat{\rho}_A^0 = \exp[-\beta\hat{H}_A]/Z_A^0(\beta)$, where \hat{H}_A is the Hamiltonian of the main system and $\beta = 1/k_B T$ represents the inverse temperature, with k_B being the Boltzmann constant. Various thermodynamic variables of the main system can be computed from the partition function (PF), which is defined as $Z_A^0(\beta) = \text{tr}_A\{\exp[-\beta\hat{H}_A]\}$.^{1,2}

While conventional statistical mechanics is concerned with equilibrium states, nonequilibrium statistical mechanics has been developed to deal with the irreversible dynamics of a system toward thermal equilibrium states.^{3–5} The key feature of this approach is the introduction of a harmonic heat bath, which is modeled by an infinite number of harmonic oscillators in the canonical distribution $\hat{\rho}_B^0 = \exp[-\beta\hat{H}_B]/Z_B^0(\beta)$, where \hat{H}_B is the heat bath Hamiltonian and $Z_B^0(\beta) = \text{tr}_B\{\exp[-\beta\hat{H}_B]\}$. In this model, it is important to have an explicit treatment of the system–bath (SB) interaction, with the corresponding Hamiltonian being denoted by \hat{H}_I in the rest of this paper.

Such a treatment is particularly important in the quantum case because, in microscopic systems, the energy of the SB interaction cannot be neglected and the quantum coherence due to the SB interaction characterizes the quantum nature of the dynamics. Under these conditions, the thermal equilibrium state of the total system is not the product of the system and bath equilibrium states, namely, $\hat{\rho}_{tot}^{eq} = \hat{\rho}_A^{eq} \otimes \hat{\rho}_B^{eq}$, but is instead an entangled state of the system and bath described by $\hat{\rho}_{tot}^{eq} = \exp[-\beta\hat{H}_{tot}]/Z_{tot}(\beta)$, where the total Hamiltonian \hat{H}_{tot} includes \hat{H}_I , and $Z_{tot}(\beta) = \text{tr}\{\exp[-\beta\hat{H}_{tot}]\}$. Because the bath has an infinite number of degrees of freedom, direct evaluation of $Z_{tot}(\beta)$ is not easy, except in the case of a harmonic system with bilinear SB interaction.⁶

To extend the description to a generic model of this kind, Feynman–Vernon influence functional theory,^{7,8} which reduces the bath degrees of freedom through functional integration, allows us to describe the thermodynamics and dynamic properties of the reduced system accurately. Therefore, influence functional theory has become the foundation for conducting thermodynamic investigations in a variety of problems.^{9–17}

Among a variety of formalisms, the hierarchical equations of motion (HEOM) approach has proved to have broad applicability^{18,19} for a system described in both discretized energy space²⁰ and Wigner space²¹ under nonperturbative and non-Markovian SB interactions.^{22–25} Within this formalism, the

imaginary-time evolution can also be computed as a definite integral along complex-time planes.^{20,21} Although the construction of a hierarchy in the real-time formalism is well established, and a wide variety of problems have been investigated, such investigations have not been conducted in any detail in the imaginary-time case.

In this paper, we present a more detailed discussion of imaginary-time HEOM (imHEOM). We also introduce an additional BD-imHEOM that are obtained from the derivative of the elements of imHEOM with respect to inverse temperature β . We use both imHEOM and BD-imHEOM to evaluate the thermodynamic properties of not only the reduced system but also the system–bath interaction and the bath, in a numerically rigorous manner. In addition, we introduce the polyharmonic decomposition (PHD) method^{26–28} to construct both the imHEOM and the BD-imHEOM in a concise hierarchical structure that makes it possible to improve the numerical performance with high precision.

The rest of this paper is organized as follows: In Sec. II, we introduce the influence functional formalism for the thermal equilibrium state. In Sec. III, we present the derivation of the imHEOM and BD-imHEOM with the use of the PHD method. We also describe a scheme to calculate various thermodynamic variables based on the imHEOM theory. Numerical demonstrations for a spin-boson system and a 2×2 antiferromagnetic triangular spin lattice system with Ohmic spectral distribution are presented in Sec. IV. Section V is devoted to our conclusions.

II. INFLUENCE FUNCTIONAL FORMALISM FOR EQUILIBRIUM STATE

A. System–bath model

We consider a system described by a total Hamiltonian expressed as

$$\hat{H}_{tot} = \hat{H}_A + \hat{H}_I + \hat{H}_B, \quad (1)$$

where \hat{H}_A denotes the reduced system. The heat bath is modeled by an ensemble of harmonic oscillators,

$$\hat{H}_B = \sum_j^N \left(\frac{\hat{p}_j^2}{2m_j} + \frac{1}{2} m_j \omega_j^2 \hat{x}_j^2 \right), \quad (2)$$

where \hat{p}_j , \hat{x}_j , m_j , and ω_j are the momentum, position, mass, and frequency of the j th oscillator, respectively. The SB interaction is given by

$$\hat{H}_I = -\hat{V} \sum_j^N g_j \hat{x}_j, \quad (3)$$

where \hat{V} is the system part of the interaction and g_j is the j th coupling constant. The heat bath is characterized by the spectral distribution function (SDF),

$$J(\omega) \equiv \sum_j^N \frac{\hbar g_j^2}{2m_j \omega_j} \delta(\omega - \omega_j), \quad (4)$$

and the inverse temperature β .

Next, we define the reduced partition function (RPF) as

$$Z_A^{rd}(\beta) = \frac{Z_{tot}(\beta)}{Z_B^0(\beta)}. \quad (5)$$

In the case of a weak interaction, the RPF is solely determined by the canonical distribution of the system part alone, $Z_A^{rd}(\beta) \simeq Z_A^0(\beta)$, which is consistent with statistical physics. However, because $Z_A^{rd}(\beta)$ also involves the SB interaction, rigorous evaluation is limited to cases for which the main system is described by a harmonic potential or the SB interaction is treated as a second-order perturbation, where the quantum nature of the heat bath does not play a major role.^{29–31}

To evaluate Eq. (5), we define a reduced partition operator as

$$\hat{\sigma}_A^{rd}(\beta) = \frac{1}{Z_B^0(\beta)} \text{tr}_B \left\{ e^{-\beta \hat{H}_{tot}} \right\}, \quad (6)$$

which implies that $Z_A^{rd}(\beta) = \text{tr}_A \{ \hat{\sigma}_A^{rd}(\beta) \}$. In the path integral approach, we can eliminate the heat bath degrees of freedom and express Eq. (6) as^{6–10}

$$\sigma_A^{rd}(q, q', \beta \hbar) = \int_{q(0)=q'}^{q(\beta \hbar)=q} \mathcal{D}[q(\cdot)] e^{-S_A[q, \beta \hbar]} \mathcal{F}[q, \beta \hbar], \quad (7)$$

where $\{q\}$ represents a functional of the system coordinates or eigenstates, and

$$S_A[q, \beta \hbar] = \frac{1}{\hbar} \int_0^{\beta \hbar} d\tau' H_A(\tau'), \quad (8)$$

is the Euclidean action of the system Hamiltonian. The imaginary-time influence functional is expressed as $\mathcal{F}[q, \beta \hbar] = \exp\{\Phi[q, \beta \hbar]\}$, where $\Phi[q, \beta \hbar]$ is the influence phase defined as^{6–10,20,21}

$$\Phi[q, \beta \hbar] = \frac{1}{\hbar^2} \int_0^{\beta \hbar} d\tau' \int_0^{\tau'} d\tau'' V(\tau') V(\tau'') C(\tau' - \tau''), \quad (9)$$

with $V(\tau) \equiv V[q(\tau)]$, and the correlation function,

$$C(\tau) = \frac{1}{\pi} \int_0^\infty d\omega J(\omega) \left[\coth\left(\frac{\beta \hbar \omega}{2}\right) \cosh(\omega \tau) - \sinh(\omega \tau) \right]. \quad (10)$$

As in the real-time case, the term with $\coth(\beta \hbar \omega / 2) \cosh(\omega \tau)$ describes the thermal fluctuation from the bath, while $-\sinh(\omega \tau)$ describes the dissipation to the bath. The temperature-dependent factor arises from the mean of the j th bath coordinate, $\langle \hat{x}_j^2 \rangle = \coth(\beta \hbar \omega_j / 2) / (2m_j \omega_j)$, and $\hat{V} g_j \langle \hat{x}_j^2 \rangle$ represents the thermal energy supplied by the bath.

III. HIERARCHICAL EQUATIONS OF MOTION FOR EQUILIBRIUM STATE

A. Imaginary-time HEOM (imHEOM)

The elements of $\hat{\sigma}_A^{rd}(\beta)$ can be evaluated under the imHEOM approach. To construct the hierarchy, we first introduce a set of functions $\{\phi_k(\tau)\}$ that satisfy a closed differential equation,

$$\frac{\partial}{\partial \tau} \phi_k(\tau) = \sum_j^K D_{k,j} \phi_j(\tau). \quad (11)$$

The correlation function (10) is then expanded in terms of $\phi_k(\tau)$ as

$$C(\tau) = \sum_k^K \lambda_k c_k \phi_k(\tau). \quad (12)$$

Next, we replace the $\beta\hbar$ in Eq. (7) that appears as the upper limit of the imaginary-time integrals in Eqs. (8) and (9) by $\tau \in [0, \beta]$, while leaving $\coth(\beta\hbar\omega/2)$ in Eq. (10) unchanged. The imHEOM are obtained by differentiating $\hat{\sigma}_A^{rd}(q, q', \tau)$ with respect to τ as^{20,21} (see Appendix A)

$$\begin{aligned} \frac{\partial}{\partial \tau} \hat{\sigma}_{[\bar{n}]}(\tau) &= -\hat{H}_A \hat{\sigma}_{[\bar{n}]}(\tau) + \sum_k^K \lambda_k \hat{V} \hat{\sigma}_{[\bar{n}+\bar{e}_k]}(\tau) \\ &+ \sum_k^K n_k c_k \phi_k(0) \hat{V} \hat{\sigma}_{[\bar{n}-\bar{e}_k]}(\tau) \\ &+ \sum_{k,j}^K n_k \frac{c_k D_{k,j}}{c_j} \hat{\sigma}_{[\bar{n}-\bar{e}_k+\bar{e}_j]}(\tau), \end{aligned} \quad (13)$$

where \bar{e}_k is the k th unit vector.

To obtain the RPF defined as in Eq. (5), we integrate Eq. (13) from $\tau = 0$ to β with the initial condition $\hat{\sigma}_{[\bar{0}]}(\tau = 0) = \mathbf{I}_A$, where \mathbf{I}_A is the unit matrix. Thus, we have

$$Z_A^{rd}(\beta) = \text{tr}_A \left\{ \hat{\sigma}_{[\bar{0}]}(\beta) \right\}. \quad (14)$$

Various thermodynamic quantities can be obtained from $Z_A^{rd}(\beta)$. For example, the reduced Helmholtz free energy is evaluated as

$$F_A^{rd}(\beta) = -\frac{1}{\beta} \ln Z_A^{rd}(\beta). \quad (15)$$

From Eq. (5), we also have

$$F_{tot}(\beta) = F_A^{rd}(\beta) + F_B^0(\beta), \quad (16)$$

where $F_{tot}(\beta) \equiv -\ln Z_{tot}(\beta)/\beta$ and $F_B^0(\beta) \equiv -\ln Z_B^0(\beta)/\beta$. Although $F_B^0(\beta)$ is a divergent function regardless of β , this is not a hindrance because $F_{tot}(\beta)$ is a state variable that can be defined by the value with or without external perturbation. Therefore, for the perturbed system denoted by A' , the change in the total free energy is expressed as

$$\Delta F_{tot}(\beta) = \Delta F_A^{rd}(\beta), \quad (17)$$

where $\Delta F_A^{rd}(\beta) = F_A^{rd}(\beta) - F_A^{rd}(\beta)$. Note that if the system is in a quasi-static equilibrium state, the above equality does not hold because heat is generated in the system.^{24,25}

The reduced internal energy and reduced entropy are obtained as

$$\begin{aligned} U_A^{rd}(\beta) &= -\frac{\partial}{\partial \beta} \ln Z_A^{rd}(\beta) \\ &= -\frac{1}{Z_A^{rd}(\beta)} \text{tr}_A \left\{ \frac{\partial}{\partial \beta} \hat{\sigma}_A^{rd}(\beta) \right\} \end{aligned} \quad (18)$$

and

$$S_A^{rd}(\beta) = \beta^2 \frac{\partial}{\partial \beta} F_A^{rd}(\beta). \quad (19)$$

They satisfy the relation:

$$S_A^{rd}(\beta) = \beta \left[U_A^{rd}(\beta) - F_A^{rd}(\beta) \right], \quad (20)$$

which is equivalent to $S_{tot}(\beta) = \beta [U_{tot}(\beta) - F_{tot}(\beta)]$.

B. Polyharmonic decomposition (PHD) method

The imHEOM were originally constructed based on a Fourier series in terms of the Matsubara frequencies.^{20,21} However, this scheme has slow convergence and requires a large number of hierarchical elements, particularly at low temperatures. To reduce the numerical cost, in this work, we adopt the PHD method, which represents a nonperiodic and holomorphic function $F(x)$ as^{26,27}

$$F(x) = \sum_{q=0}^{Q-1} F_{0,q} f_{0,q}(x) + \sum_{l=1}^L F_l f_l(x), \quad (21)$$

where $x \in (0, 1)$, Q and L are positive integers that represent the order of expansion, and $f_{0,q}(x) = P_q(2x-1)$ is the q th Legendre polynomial. The coefficients are given by

$$F_{0,q} = (2q+1) \int_0^1 dx F(x) f_{0,q}(x), \quad (22)$$

$$F_l = 2 \int_0^1 dx F(x) f_l(x). \quad (23)$$

Originally, $f_l(x)$ was expressed as a sum of complex-valued exponential functions, whose coefficients had to be determined by diagonalizing specified matrices. Here, to simplify the calculation while maintaining accuracy, we employ an asymptotic approximation,²⁷

$$f_l(x) = \cos(\alpha_l x + \theta), \quad (24)$$

with parameters given by

$$\alpha_l = \frac{2l+Q-1}{2} \pi, \quad \theta = \frac{Q-1}{4} \pi. \quad (25)$$

To apply these to the imHEOM, we set $x = \tau/\beta$ and substitute Eq. (23) into Eq. (10). Integrating over ω , we now express $C(\tau)$ as

$$C(\tau) = \sum_{q=0}^{Q-1} \lambda_{q+1} c_{0,q} \phi_{0,q}(\tau) + \sum_{l=1}^L \lambda_{Q+l} c_l \phi_l(\tau), \quad (26)$$

where $\lambda_n = [1 - (-1)^n]/2$ for any positive integer n . The basis functions are given by

$$\phi_{0,q}(\tau) = P_q \left(\frac{2\tau}{\beta} - 1 \right), \quad (27)$$

$$\phi_l(\tau) = \cos \left(\frac{\alpha_l}{\beta} \tau + \theta \right). \quad (28)$$

The first derivatives of the above functions are further decomposed into the same function set $\{\phi_k(\tau)\}$ to satisfy Eq. (11). In this way, we construct the imHEOM based on the PHD. The numerical accuracy of the PHD scheme is verified in Appendix B.

The key to the PHD method lies in the exponential function $\exp(-\omega\tau)$. However, due to the integration with respect to ω in Eq. (10), the numerical accuracy of the PHD method is reduced in the region of $\omega \ll 1/\beta\hbar$ and $\omega \gg 1/\beta\hbar$, where the function asymptotically approaches a constant. To improve accuracy, we introduce here the cut-off frequencies ω_{\min} and ω_{\max} for $\beta\hbar\omega_{\min} \ll 1$ and $\beta\hbar\omega_{\max} \gg 1$ and divide the integration in Eq. (10) as follows:

$$\int_0^\infty d\omega \rightarrow \int_0^{\omega_{\min}} d\omega + \int_{\omega_{\min}}^{\omega_{\max}} d\omega + \int_{\omega_{\max}}^\infty d\omega. \quad (29)$$

The first and last terms are then solved analytically using appropriate approximations, while the second term is evaluated using the PHD method.

C. The β -derivative imaginary-time HEOM (BD-imHEOM) for internal energy calculation

The internal energy can be evaluated from Eq. (18) using a finite-difference expression for $Z_A^{rd}(\beta)$ with respect to β . Instead, we introduce a more straightforward approach by deriving a new set of equations for $\partial\hat{\sigma}_A^{rd}(\beta)/\partial\beta$ in Eq. (18). Using the definition in Eq. (7), we can evaluate the derivative with respect to β as

$$\begin{aligned} & \frac{\partial}{\partial\beta} \left(e^{-S_A[q,\beta\hbar]} e^{\Phi[q,\beta\hbar]} \right) \\ &= \left\{ -\frac{1}{\hbar} H_A(\beta\hbar) + \frac{1}{\hbar^2} V(\beta\hbar) \int_0^{\beta\hbar} d\tau'' V(\tau'') C(\beta\hbar - \tau'') \right. \\ & \quad \left. + \Psi[q,\beta\hbar] \right\} e^{-S_A[q,\beta\hbar]} e^{\Phi[q,\beta\hbar]}, \end{aligned} \quad (30)$$

where

$$\Psi[q,\tau] = \frac{1}{\hbar^2} \int_0^\tau d\tau' \int_0^{\tau'} d\tau'' V(\tau') V(\tau'') \partial_\beta C(\tau' - \tau''), \quad (31)$$

and

$$\frac{\partial C(\tau)}{\partial\beta} = -\frac{1}{\pi} \int_0^\infty d\omega J(\omega) \frac{\hbar\omega}{2 \sinh^2\left(\frac{\beta\hbar\omega}{2}\right)} \cosh(\omega\tau) \quad (32)$$

can be regarded as the heat capacity of the bath as a function of the inverse temperature. Using the definitions of the hierarchical elements, we have

$$\frac{\partial}{\partial\beta} \hat{\sigma}_A^{rd}(\beta\hbar) = -\hat{H}_A \hat{\sigma}_{[0]}(\beta\hbar) + \sum_k^K \hat{V} \hat{\sigma}_{[\bar{e}_k]}(\beta\hbar) + \zeta_A^{rd}(\beta\hbar), \quad (33)$$

where the density matrix elements of the last term at τ are defined as

$$\zeta_A^{rd}(q, q', \tau) = \int_{q(0)=q'}^{q(\tau)=q} \mathcal{D}[q(\cdot)] e^{-S_A[q,\tau]} \mathcal{F}[q, \tau] \Psi[q, \tau]. \quad (34)$$

To evaluate $\zeta_A^{rd}(\beta\hbar)$, we derive the BD-imHEOM for the hierarchical elements involving Eq. (32). Using the PHD method, we have

$$\frac{\partial C(\tau)}{\partial\beta} = \sum_k^K c_k' \phi_k(\tau). \quad (35)$$

The BD-imHEOM are then expressed as (see Appendix A)

$$\begin{aligned} \frac{\partial}{\partial\tau} \hat{\zeta}_{[\bar{n}]}(\tau) &= -\hat{H}_A \hat{\zeta}_{[\bar{n}]}(\tau) + \sum_k^K \hat{V} \hat{\zeta}_{[\bar{n}+\bar{e}_k]}(\tau) \\ & \quad + \sum_k^K n_k c_k \phi_k(0) \hat{V} \hat{\zeta}_{[\bar{n}-\bar{e}_k]}(\tau) \\ & \quad + \sum_{k,j}^K \frac{n_k c_k D_{kj}}{c_j} \hat{\zeta}_{[\bar{n}-\bar{e}_k+\bar{e}_j]}(\tau) \\ & \quad + \sum_k^K \frac{c_k'}{c_k} \hat{V} \hat{\sigma}_{[\bar{n}+\bar{e}_k]}(\tau). \end{aligned} \quad (36)$$

We integrate Eq. (13) and the above equations simultaneously over $\tau \in (0, \beta\hbar)$ with the initial condition $\hat{\zeta}_{[0]}(\tau=0) = 0$. We then evaluate the internal energy of the system and the SB interaction as

$$\begin{aligned} U_A(\beta) &= \langle \hat{H}_A \rangle \\ &= \text{tr}_A \left\{ \hat{H}_A \frac{\hat{\sigma}_{[0]}(\beta)}{Z_A^{rd}(\beta)} \right\} \end{aligned} \quad (37)$$

and

$$\begin{aligned} U_I(\beta) &= \langle \hat{H}_I \rangle \\ &= -\sum_k^K \text{tr}_A \left\{ \hat{V} \frac{\hat{\sigma}_{[\bar{e}_k]}(\beta)}{Z_A^{rd}(\beta)} \right\}, \end{aligned} \quad (38)$$

where $\langle \dots \rangle$ represents the thermodynamic average of the total system. The above results are consistent with the expressions obtained from the real-time HEOM.^{22,23,32} The internal energy of the heat bath is evaluated using the solution of Eq. (36) as

$$\begin{aligned} U_B(\beta) &= \langle \hat{H}_B \rangle \\ &= -\text{tr}_A \left\{ \frac{\hat{\zeta}_{[0]}(\beta)}{Z_A^{rd}(\beta)} \right\} + U_B^0(\beta). \end{aligned} \quad (39)$$

The total internal energy $U_{tot}(\beta) = U_A^{rd}(\beta) + U_B^0(\beta)$ is now expressed as

$$U_{tot}(\beta) = U_A(\beta) + U_I(\beta) + U_B(\beta). \quad (40)$$

Through the use of the BD-imHEOM, we can evaluate the contributions to the internal energy from each part of the Hamiltonian separately.

IV. NUMERICAL RESULTS

In this section, we report the results of numerical simulations that demonstrate the validity and applicability of the present approach.

A. Spin-boson system

We first investigate the changes in internal energy for thermal transitions between isothermal and adiabatic states of the total system. With regard to the isothermal state, we consider the Hamiltonian

$$\hat{H}_{tot}(g) = \hat{H}_A + g \hat{H}_I + \hat{H}_B, \quad (41)$$

where $g \in (0, 1)$ is a dimensionless factor representing the strength of the coupling between system and heat bath. The PF is then expressed as

$$Z_{tot}(g, \beta) = \text{tr} \left\{ e^{-\beta \hat{H}_{tot}(g)} \right\}. \quad (42)$$

The adiabatic state is described by the case $f = 0$, with a factorized form of the PF, $Z_{tot}(0, \beta) = Z_A^0(\beta) Z_B^0(\beta)$. Thus, the change in the total PF is expressed as

$$\Delta Z_{tot}(g, \beta) = \frac{Z_A^{rd}(g, \beta)}{Z_A^0(\beta)}, \quad (43)$$

where $Z_A^0(\beta)$ is evaluated from the eigenstates of the system Hamiltonian. Using $Z_A^0(\beta)$, we can calculate the free energy $F_A^0(\beta)$, internal energy $U_A^0(\beta)$, and entropy $S_A^0(\beta)$ of the system. The change in the total free energy is now given by

$$\Delta F_{tot}(g, \beta) = F_A^{rd}(g, \beta) - F_A^0(\beta), \quad (44)$$

where $F_A^{rd}(g, \beta)$ is obtained from Eq. (15) using the imHEOM. Accordingly, the change in the internal energy is evaluated as

$$\Delta U_{tot}(g, \beta) = U_A^{rd}(g, \beta) - U_A^0(\beta), \quad (45)$$

where $U_A^{rd}(g, \beta)$ is obtained from Eqs. (18) and (33) through use of the BD-imHEOM. From Eq. (20), we can evaluate the change in the entropy as

$$\Delta S_{tot}(g, \beta) = S_A^{rd}(g, \beta) - S_A^0(\beta). \quad (46)$$

We now conduct our numerical computations for a simple spin-boson system, with

$$\hat{H}_A = \frac{\hbar\omega_0}{2} \hat{s}^z + \frac{\hbar\Delta}{2} \hat{s}^x, \quad (47)$$

where \hat{s}^z and \hat{s}^x are the spin operators in the z and x directions, and Δ represents the strength of the transverse external field. The SB interaction, Eq. (3), is given by

$$\hat{V} = \hat{s}^x. \quad (48)$$

We then chose ω_0 as the unit for all other variables and set $\Delta = \omega_0$. The SDF is chosen as the Ohmic form with an exponential cutoff,

$$\mathcal{J}_O(\omega) = \frac{\zeta}{\gamma} e^{-\frac{|\omega|}{\gamma}}, \quad (49)$$

where ζ is the dimensionless coupling strength and γ is the cutoff frequency. Here, we choose $\zeta = 0.5\omega_0$ and $\gamma = \omega_0$. The decomposition parameter values are set as $Q = 2$ and $L = 10-20$. The truncation of the hierarchy level is $N \leq 10$. Moreover, we use only auxiliary operators that satisfy $\prod_k^K |c_k| > 10^{-10}$ for calculation (see Appendix B). We numerically integrate the imHEOM and BD-imHEOM using the fourth-order low-storage Runge-Kutta method (LSRK4), with the imaginary-time step $\delta\tau = 10^{-4}(\omega_0^{-1})$.

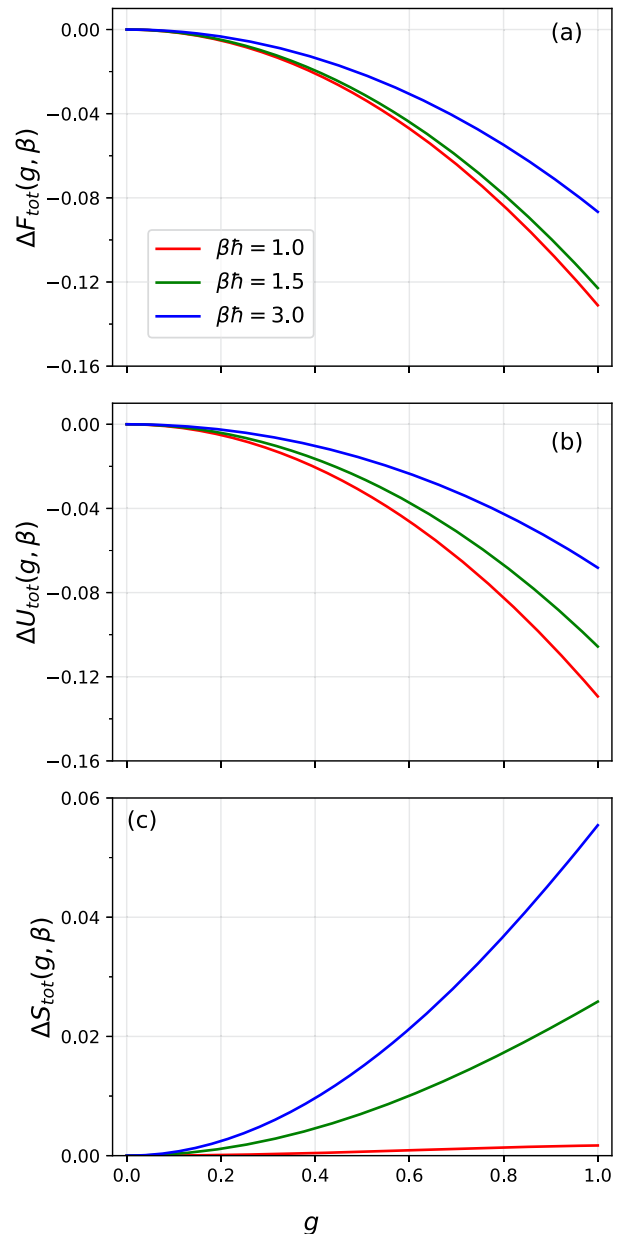


FIG. 1. The change in the (a) free energy, (b) internal energy, and (c) entropy as a function of g . The red, green, and blue curves represent different temperature cases.

Figures 1(a)–1(c) illustrate the changes in the free energy $\Delta F_{tot}(g, \beta)$, internal energy $\Delta U_{tot}(g, \beta)$, and entropy $\Delta S_{tot}(g, \beta)$, respectively, from the adiabatic state to the isothermal state at fixed inverse temperatures. The changes in free energy and internal energy are decreasing functions of g , whereas the change in entropy is an increasing function. This is because as g increases, the excitation energy of the system also increases due to the presence in H_I of the operator \hat{V} . In this example of an adiabatic–isothermal transition, $g\hat{H}_I$ can be regarded as the work done for the entire system to insert the adiabatic wall. Thus, the entropy production $\Delta S_{tot}(g, \beta)$ is always positive, and it is larger for lower temperatures. We should note that the difference in thermodynamic quantities between the adiabatic state and the isothermal state is useful for validating the simulation when the reduced system is infinite while the heat bath is comparatively small.^{33,34}

B. A 2×2 antiferromagnetic triangular Ising system with transverse field

Next, we demonstrate the scalability of this approach. For this purpose, we employ the 2×2 transverse Ising model. The system Hamiltonian is defined as^{35,36}

$$\hat{H}_A = -J \sum_{\langle ij \rangle} \hat{s}_i^z \hat{s}_j^z - \mu \sum_i \hat{s}_i^x, \quad (50)$$

where J is the interaction between nearest-neighbor pairs $\langle i, j \rangle$ and μ represents the transverse field. To conduct the numerical calculation, we choose an antiferromagnetic case $J = -0.5\omega_0$. The system part of the SB interaction has the same form as in the transverse field and is expressed as

$$\hat{V} = \sum_i \hat{s}_i^x. \quad (51)$$

The SDF is chosen as that in Eq. (49), with $\zeta = 0.1\omega_0$ and $\gamma = \omega_0$ fixed. The other parameter values for the hierarchy and the PHD decomposition are the same as in Sec. IV A.

Each component of the internal energy is obtained from Eqs. (37)–(39). In addition to these, we calculate the heat capacity defined as $C_\alpha \equiv \partial U_\alpha(\beta) / \partial \beta$. The derivatives of the internal energy with respect to β for $\alpha = A, I$, and B are evaluated by the first-order finite-difference method as

$$C_\alpha(\beta) = \lim_{\delta\beta \rightarrow 0} \frac{U_\alpha(\beta + \delta\beta) - U_\alpha(\beta)}{\delta\beta} \quad (52)$$

with $\delta\beta = 10^{-4} - 10^{-3}$ (ω_0^{-1}).

Figures 2(a)–2(c) depict the internal energy of the system $U_A(\beta)$, that of the SB interaction $U_I(\beta)$, and that of the heat bath $\Delta U_B(\beta) = U_B(\beta) - U_B^0(\beta)$ as functions of $\beta\hbar$ for $\mu = 0.1, 0.3$, and 0.5 . The system's internal energy $U_A(\beta)$ decreases monotonically as β increases because thermal excitation is suppressed. Moreover, the value of $U_A(\beta)$ becomes smaller for larger μ because the transverse field enhances the excitation energies of the spin lattice system. Such a tendency is also observed in an isolated system where there is no interaction with a heat bath.

The absolute values of $U_I(\beta)$ correspond to the strength of the SB interaction. As shown in Figs. 2(b) and 2(c), $U_I(\beta)$ and $\Delta U_B(\beta)$ roughly exhibit an opposite β dependence. This is because, as a consequence of Eq. (16), the internal energy of the total system is the

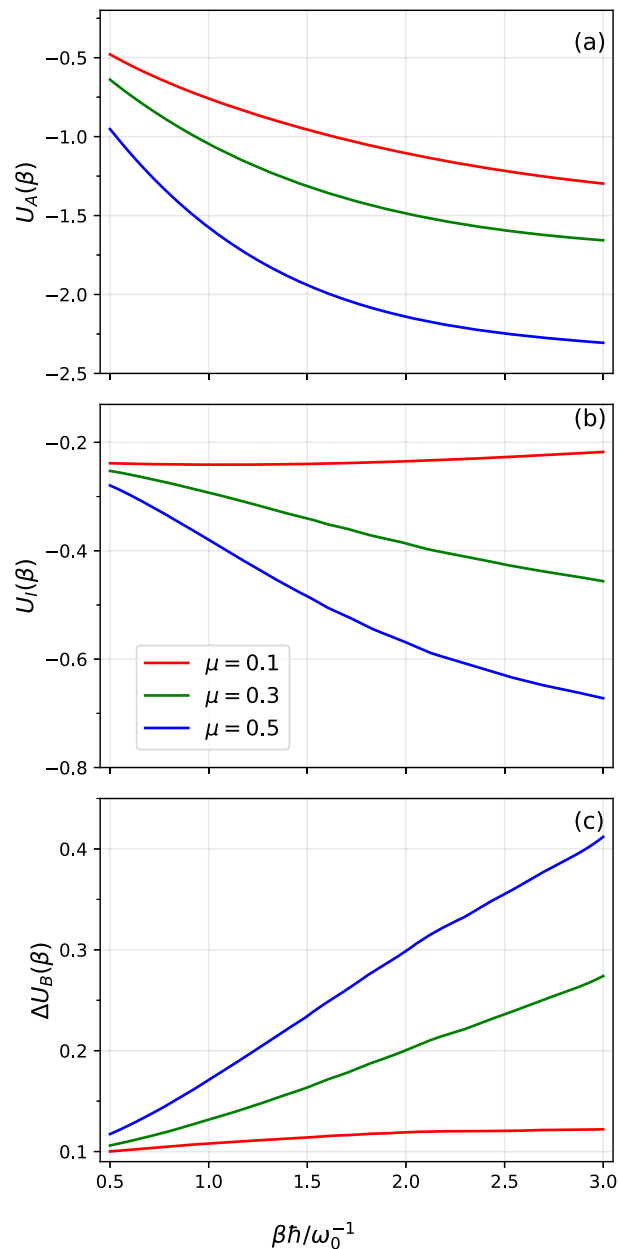


FIG. 2. The internal energy of the (a) system, (b) SB interaction, and (c) heat bath are plotted as a function of $\beta\hbar$ for a weak SB coupling case. The colored curves represent the results for different transverse field strength cases: $\mu = 0.1$ (red curve), $\mu = 0.3$ (green curve), and $\mu = 0.5$ (blue curve).

same as the internal energy of the reduced system. Because we set \hat{V} parallel to the transverse field, $U_I(\beta)$ and $\Delta U_B(\beta)$ become almost flat for small μ , as shown in Figs. 2(b) and 2(c).

In Figs. 3(a)–3(c), we plot the heat capacity $C_\alpha(\beta)$ for $\alpha = A, I$, and B corresponding to the cases in Figs. 2(a)–2(c), respectively. The heat capacity of the system, $C_A(\beta)$, exhibits a maximum near the inverse temperature corresponding to the excitation energy. As a result, the position of the maximum shifts in

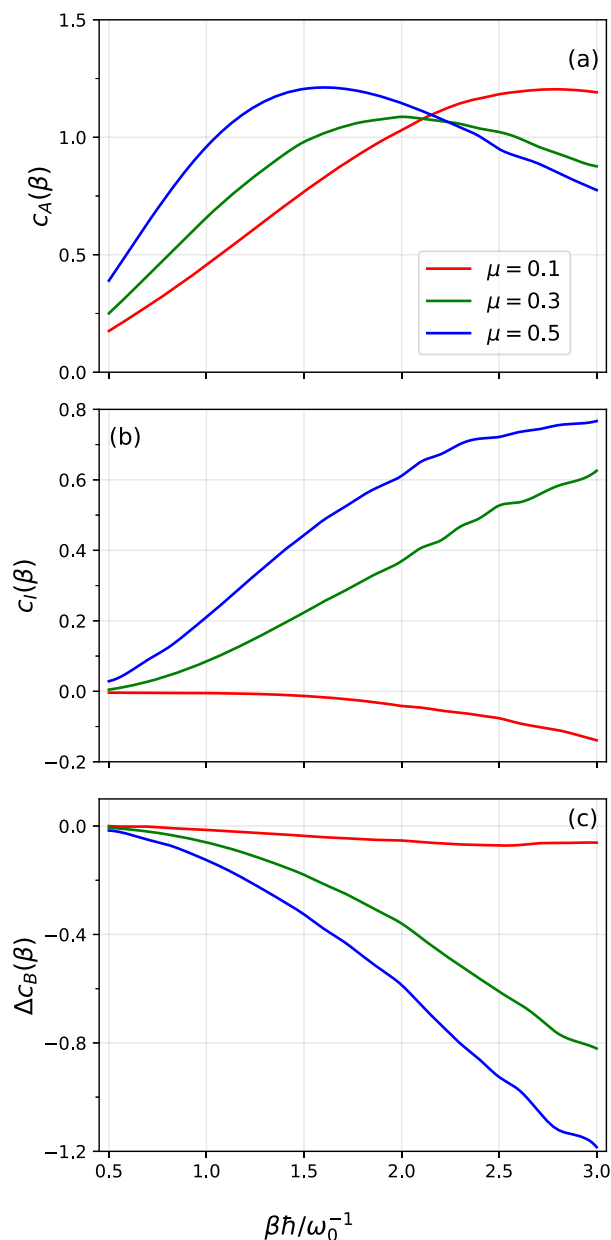


FIG. 3. The heat capacity of the (a) system, (b) SB interaction, and (c) heat bath are plotted as a function of $\beta\hbar$. The colored curves represent the results for different transverse field strength cases.

the high-temperature direction for larger μ . Because $U_I(\beta)$ and $\Delta U_B(\beta)$ exhibit monotonic behavior, $C_I(\beta)$ and $C_B(\beta)$ also behave monotonically.

The change in the internal energy of the system from the adiabatic to isothermal states is presented in Appendix C. The differences in thermodynamic quantities between these two states are useful for validating the simulation of an isolated infinite system with a small coupled heat bath.^{33,34}

V. CONCLUSIONS

The imHEOM provide a formalism for studying the thermodynamic properties of open quantum mechanical systems based on partition functions. In this paper, we have extended the imHEOM formalism and derived the so-called BD-imHEOM to solve for the temperature gradient. Numerical solution of the imHEOM enables evaluation of the thermodynamic variables of the system and the system-bath interaction, while solution of the BD-imHEOM enables evaluation of those for the heat bath. We have also introduced the PHD method to perform numerical calculations with both approaches more concisely and efficiently.

The capability of this formalism has been verified through numerical demonstrations. We have employed a spin-boson model and a 2×2 transverse Ising model to clearly reveal the behavior of various quantities in a straightforward manner. Although this work has been restricted to an Ohmic form of the SDF, we note here that the PHD method imposes no restrictions on the SDF and could have broader applications. Other forms, for example, sub-Ohmic and super-Ohmic, can also be treated, as long as the solutions for $\omega < \omega_l$ and $\omega > \omega_u$ are properly constructed. Moreover, our analysis can also be extended to a system described by Wigner distribution functions. On this basis, we can investigate not only quantum cases but also classical cases by taking the classical limits.

To make the present approach more useful, further computational efforts will have to be made to treat larger systems. For example, we can extend our imHEOM to the wavefunction-based case by utilizing some other techniques, such as the stochastic hierarchy of pure states (HOPS),³⁷ the stochastic Schrödinger equation (SSE),³⁸ the hierarchical stochastic Schrödinger equations (HSSE),³⁹ and the hierarchical Schrödinger equations of motion (HSEOM).^{33,34} The scalability of all the above-mentioned approaches is the same as that of the typical Schrödinger equation, which incurs less computational cost than the density-matrix-based approach. We believe that the present results clarify the key features of quantum open dynamics systems with regard to their fundamental thermodynamic properties.

ACKNOWLEDGMENTS

Y.T. was supported by the JSPS KAKENHI (Grant No. B 21H01884).

AUTHOR DECLARATIONS

Conflict of Interest

The authors have no conflicts to disclose.

DATA AVAILABILITY

The data that support the findings of this study are available from the corresponding authors upon reasonable request.

APPENDIX A: DERIVATION OF imHEOM AND BD-imHEOM

In this appendix, we illustrate the derivation of the imHEOM and BD-imHEOM. The path integral representation of the reduced density matrix elements at τ is expressed as

$$\sigma_A(q, q', \tau) = \int_{q(0)=q'}^{q(\tau)=q} \mathcal{D}[q(\cdot)] e^{-S_A[q, \tau]} e^{\Phi[q, \tau]}. \quad (\text{A1})$$

Employing the linear summation (12), we can rewrite Eq. (9) as

$$\begin{aligned} \Phi[q, \tau] &= \frac{1}{\hbar^2} \int_0^\tau d\tau' \int_0^{\tau'} d\tau'' V(\tau') V(\tau'') C(\tau' - \tau'') \\ &= \sum_k^K \frac{\lambda_k}{\hbar^2} \int_0^\tau d\tau' \int_0^{\tau'} d\tau'' V(\tau'') \Theta_k(\tau', \tau''), \end{aligned} \quad (\text{A2})$$

where

$$\Theta_k(\tau', \tau'') = c_k \phi_k(\tau' - \tau'') V(\tau''). \quad (\text{A3})$$

To obtain the imHEOM, we introduce the following set of auxiliary operators:

$$\begin{aligned} \sigma_{[\vec{n}]}(q, q', \tau) &= \int_{q(0)=q'}^{q(\tau)=q} \mathcal{D}[q(\cdot)] e^{-S_A[q, \tau]} \mathcal{F}[q, \tau] \\ &\times \prod_k^K \left[\int_0^\tau d\tau' \Theta_k(\tau, \tau') \right]^{n_k}, \end{aligned} \quad (\text{A4})$$

where $[\vec{n}] = [\dots, n_k, \dots]$ is the index vector. Thus, the zeroth element at $\tau = \beta$ corresponds to Eq. (A1), while all of the other elements are introduced for computational purposes. Taking the partial derivative with respect to τ , we obtain Eq. (13).

Next, we derive the BD-imHEOM. We employ Eq. (35) and introduce a new set of auxiliary operators defined as

$$\begin{aligned} \varsigma_{[\vec{n}]}(q, q', \tau) &= \int_{q(0)=q'}^{q(\tau)=q} \mathcal{D}[q(\cdot)] e^{-S_A[q, \tau]} \mathcal{F}[q, \tau] \\ &\times \Psi[q, \tau] \prod_k^K \left[\int_0^\tau d\tau' \Theta_k(\tau, \tau') \right]^{n_k}. \end{aligned} \quad (\text{A5})$$

Differentiating these with respect to τ , we obtain Eq. (36).

We note that the BD-imHEOM are more sensitive to temperature changes than the imHEOM. As can be seen from Eq. (32), $\partial C(\tau)/\partial\beta$ decays exponentially with β (i.e., $\propto e^{-\beta}$). At very low temperatures (i.e., $\beta\hbar\omega_0 > 50$), however, this term becomes almost constant, and therefore, we cannot apply the PHD method directly for the BD-imHEOM in this region, while there is no such limitation on the imHEOM, as we confirmed from the numerical simulations for the case of extremely low temperature ($\beta\hbar\omega_0 \simeq 100$) and strong coupling ($\zeta \simeq 2.0\omega_0$).

APPENDIX B: NUMERICAL ACCURACY OF imHEOM

In this appendix, to verify the accuracy of the imHEOM approach and PHD method, we compare the equilibrium distribution,

$$\hat{\rho}^{im} = \frac{\delta Z_A^{rd}(\beta)}{Z_A^{rd}(\beta)}, \quad (\text{B1})$$

with that obtained from the steady-state solution of the real-time HEOM.^{40,41} We use the same spin-boson system as in Sec. IV A. The SDF is chosen in the Drude form,

$$J_D = \frac{\zeta \gamma^2 \omega}{\omega_0(\gamma^2 + \omega^2)}, \quad (\text{B2})$$

with $\gamma = \omega_0$ and $\zeta = 0.5\omega$. To conduct the numerical integration in the real-time HEOM approach, we employ the Padé decomposition method with dimension $K = 10\text{--}20$ and hierarchy truncation level $N \leq 10$. The time step for the LSRK4 method is chosen as $\delta t = 10^{-2}\omega_0^{-1}$.

The relative difference is defined as

$$\epsilon(\beta) = -\log_{10} \left| \frac{\rho_0^{re}(\beta) - \rho_0^{im}(\beta)}{\rho_0^{re}(\beta)} \right|, \quad (\text{B3})$$

where ρ_0^{re} and ρ_0^{im} are the ground-state populations obtained from the real-time and imaginary-time approaches, respectively. Figure 4 shows $\epsilon(\beta)$ for typical weak-coupling ($\zeta = 0.01$), intermediate-coupling ($\zeta = 0.1$), and strong-coupling ($\zeta = 0.5$) cases. For all cases, the deviation between the two approaches is less than 1%, which proves the accuracy of the imHEOM. Although the error becomes larger in the low-temperature and strong-coupling case, we can improve the accuracy by increasing the number of decomposition functions and the hierarchy level. We have found that to

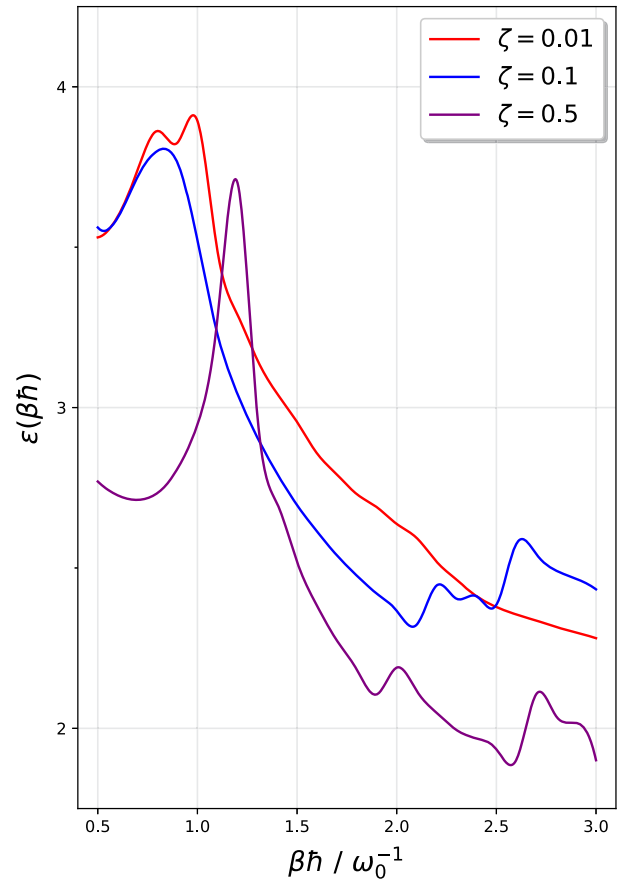


FIG. 4. The relative difference between imaginary- and real-time HEOM is shown in logarithmic scale. The red, blue, and purple curves correspond to the typical weak-, intermediate-, and strong-coupling cases, respectively.

maintain numerical accuracy, the number of hierarchies for the imHEOM with the PHD method should satisfy

$$L \simeq \begin{cases} 5\beta\hbar\omega_0 + 10 & (\beta\omega_0 < 10), \\ 10\sqrt{\beta\hbar\omega_0} & (\beta\omega_0 \geq 10). \end{cases} \quad (\text{B4})$$

Moreover, because $c_k \propto \beta^{-1}$, the deeper hierarchy elements decay rapidly to 0. Thus, to reduce the computational cost, we employ only auxiliary operators that satisfy $\prod_k^K |c_k| > 10^{-10}$. The accuracy of the numerical calculation can be adjusted easily by changing the number of hierarchical elements included in the calculation.

APPENDIX C: CHANGE IN INTERNAL ENERGY FOR 2×2 SPIN LATTICE SYSTEM

In Fig. 5, we plot the change in the system's internal energy from the adiabatic state ($H_I = 0$) to the isothermal state, defined as $\Delta U_A(\beta) = U_A(\beta) - U_A^0(\beta)$, where $U_A^0(\beta)$ is the internal energy of \hat{H}_A . The changes in the internal energies for SB interaction and the bath are identical to those shown in Figs. 2(b) and 2(c), respectively. While both $U_A(\beta)$ and $U_A^0(\beta)$ are monotonically decreasing functions, their difference $\Delta U_A(\beta)$ exhibits a minimum at larger μ . This

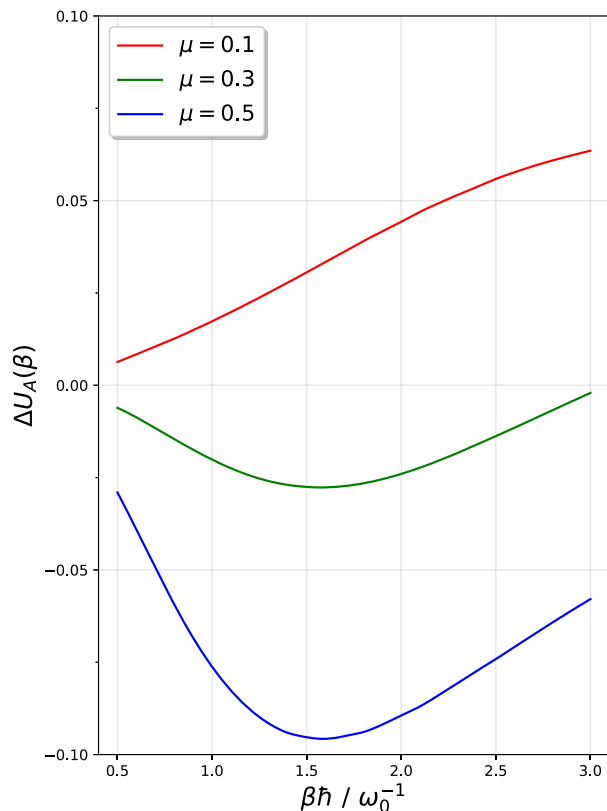


FIG. 5. The change of the system internal energy $\Delta U_A(\beta) = U_A(\beta) - U_A^0(\beta)$ is depicted as a function of inverse temperature. The colored curves represent the results for different transverse field strength cases: $\mu = 0.1$ (red curve), $\mu = 0.3$ (green curve), and (c) $\mu = 0.5$ (blue curve).

is because the curvatures of these functions are greater for larger μ , and the presence of the SB interaction further enhances the effects of μ because we have chosen μ and \hat{V} in the same direction.

REFERENCES

- R. Kubo, M. Toda, and N. Hashitsume, *Statistical Physics II* (Springer Berlin Heidelberg, 1985).
- Y. Oono, *Perspectives on Statistical Thermodynamics* (Cambridge University Press, 2017).
- U. Weiss, *Quantum Dissipative Systems*, 4th ed. (World Scientific, 2012).
- H.-P. Breuer and F. Petruccione, *The Theory of Open Quantum Systems* (Oxford University Press, Oxford, 2002), p. xxi + 625.
- P. Talkner and P. Hänggi, "Colloquium: Statistical mechanics and thermodynamics at strong coupling: Quantum and classical," *Rev. Mod. Phys.* **92**, 041002 (2020).
- H. Grabert, P. Schramm, and G.-L. Ingold, "Quantum Brownian motion: The functional integral approach," *Phys. Rep.* **168**, 115–207 (1988).
- R. P. Feynman and F. L. Vernon, "The theory of a general quantum system interacting with a linear dissipative system," *Ann. Phys.* **24**, 118–173 (1963).
- R. P. Feynman, *Statistical Mechanics* (Benjamin, Reading, MA, 1972).
- A. O. Caldeira and A. J. Leggett, "Influence of dissipation on quantum tunneling in macroscopic systems," *Phys. Rev. Lett.* **46**, 211–214 (1981).
- A. J. Leggett, S. Chakravarty, A. T. Dorsey, M. P. A. Fisher, A. Garg, and W. Zwerger, "Dynamics of the dissipative two-state system," *Rev. Mod. Phys.* **59**, 1–85 (1987).
- P. G. Wolynes, "Imaginary time path integral Monte Carlo route to rate coefficients for nonadiabatic barrier crossing," *J. Chem. Phys.* **87**, 6559–6561 (1987).
- J. Cao and G. A. Voth, "A unified framework for quantum activated rate processes. I. General theory," *J. Chem. Phys.* **105**, 6856–6870 (1996).
- J. M. Moix, Y. Zhao, and J. Cao, "Equilibrium-reduced density matrix formulation: Influence of noise, disorder, and temperature on localization in excitonic systems," *Phys. Rev. B* **85**, 115412 (2012).
- C. K. Lee, J. Moix, and J. Cao, "Accuracy of second order perturbation theory in the polaron and variational polaron frames," *J. Chem. Phys.* **136**, 204120 (2012).
- G. A. Voth, D. Chandler, and W. H. Miller, "Rigorous formulation of quantum transition state theory and its dynamical corrections," *J. Chem. Phys.* **91**, 7749–7760 (1989).
- H. Gong, Y. Wang, H.-D. Zhang, R.-X. Xu, X. Zheng, and Y. Yan, "Thermodynamic free-energy spectrum theory for open quantum systems," *J. Chem. Phys.* **153**, 214115 (2020).
- H. Gong, Y. Wang, H.-D. Zhang, Q. Qiao, R.-X. Xu, X. Zheng, and Y. Yan, "Equilibrium and transient thermodynamics: A unified dissipaton-space approach," *J. Chem. Phys.* **153**, 154111 (2020).
- Y. Tanimura, "Stochastic Liouville, Langevin, Fokker-Planck, and Master equation approaches to quantum dissipative systems," *J. Phys. Soc. Jpn.* **75**, 082001 (2006).
- Y. Tanimura, "Numerically "exact" approach to open quantum dynamics: The hierarchical equations of motion (HEOM)," *J. Chem. Phys.* **153**, 020901 (2020).
- Y. Tanimura, "Reduced hierarchical equations of motion in real and imaginary time: Correlated initial states and thermodynamic quantities," *J. Chem. Phys.* **141**, 044114 (2014).
- Y. Tanimura, "Real-time and imaginary-time quantum hierarchal Fokker-Planck equations," *J. Chem. Phys.* **142**, 144110 (2015).
- A. Kato and Y. Tanimura, "Quantum heat transport of a two-qubit system: Interplay between system-bath coherence and qubit-qubit coherence," *J. Chem. Phys.* **143**, 064107 (2015).
- A. Kato and Y. Tanimura, "Quantum heat current under non-perturbative and non-Markovian conditions: Applications to heat machines," *J. Chem. Phys.* **145**, 224105 (2016).
- S. Sakamoto and Y. Tanimura, *J. Chem. Phys.* **153**, 234107 (2020).
- S. Sakamoto and Y. Tanimura, "Open quantum dynamics theory for non-equilibrium work: Hierarchical equations of motion approach," *J. Phys. Soc. Jpn.* **90**, 033001 (2021).

- ²⁶A. Iserles and S. P. Norsett, *IMA J. Numer. Anal.* **28**, 862–887 (2008).
- ²⁷B. Adcock, *J. Approximation Theory* **163**, 1638–1674 (2011).
- ²⁸B. Adcock, “Modified Fourier expansions: Theory, construction and applications,” *Ph.D. Thesis* (University of Cambridge, 2010).
- ²⁹M. F. Gelin and M. Thoss, *Phys. Rev. E* **79**, 051121 (2009).
- ³⁰G. W. Ford and R. F. O’Connell, *Phys. Lett. A* **157**, 217–220 (1991).
- ³¹G. W. Ford, J. T. Lewis, and R. F. O’Connell, *Phys. Rev. Lett.* **55**, 2273–2276 (1985).
- ³²L. Zhu, H. Liu, W. Xie, and Q. Shi, “Explicit system-bath correlation calculated using the hierarchical equations of motion method,” *J. Chem. Phys.* **137**, 194106 (2012).
- ³³K. Nakamura and Y. Tanimura, “Hierarchical Schrödinger equations of motion for open quantum dynamics,” *Phys. Rev. A* **98**, 012109 (2018).
- ³⁴K. Nakamura and Y. Tanimura, “Open quantum dynamics theory for a complex subenvironment system with a quantum thermostat: Application to a spin heat bath,” *J. Chem. Phys.* **155**, 244109 (2021).
- ³⁵H. Nishimori and O. U. Press, *Statistical Physics of Spin Glasses and Information Processing: An Introduction*, International Series of Monographs on Physics (Oxford University Press, 2001).
- ³⁶M. Tsuchimoto and Y. Tanimura, *J. Chem. Theory Comput.* **11**, 3859–3865 (2015).
- ³⁷D. Suess, A. Eisfeld, and W. T. Strunz, “Hierarchy of stochastic pure states for open quantum system dynamics,” *Phys. Rev. Lett.* **113**, 150403 (2014).
- ³⁸K. Song, L. Song, and Q. Shi, “An alternative realization of the exact non-Markovian stochastic Schrödinger equation,” *J. Chem. Phys.* **144**, 224105 (2016).
- ³⁹Y. Ke and Y. Zhao, “Hierarchy of forward-backward stochastic Schrödinger equation,” *J. Chem. Phys.* **145**, 024101 (2016).
- ⁴⁰A. Ishizaki and Y. Tanimura, “Quantum dynamics of system strongly coupled to low-temperature colored noise bath: Reduced hierarchy equations approach,” *J. Phys. Soc. Jpn.* **74**, 3131–3134 (2005).
- ⁴¹H. Takahashi and Y. Tanimura, “Open quantum dynamics theory of spin relaxation: Application to μ SR and low-field NMR spectroscopies,” *J. Phys. Soc. Jpn.* **89**, 064710 (2020).